iScience

CellPress
OPEN ACCESS

Article

Alterations of endogenous pain-modulatory system of the cerebral cortex in the neuropathic pain

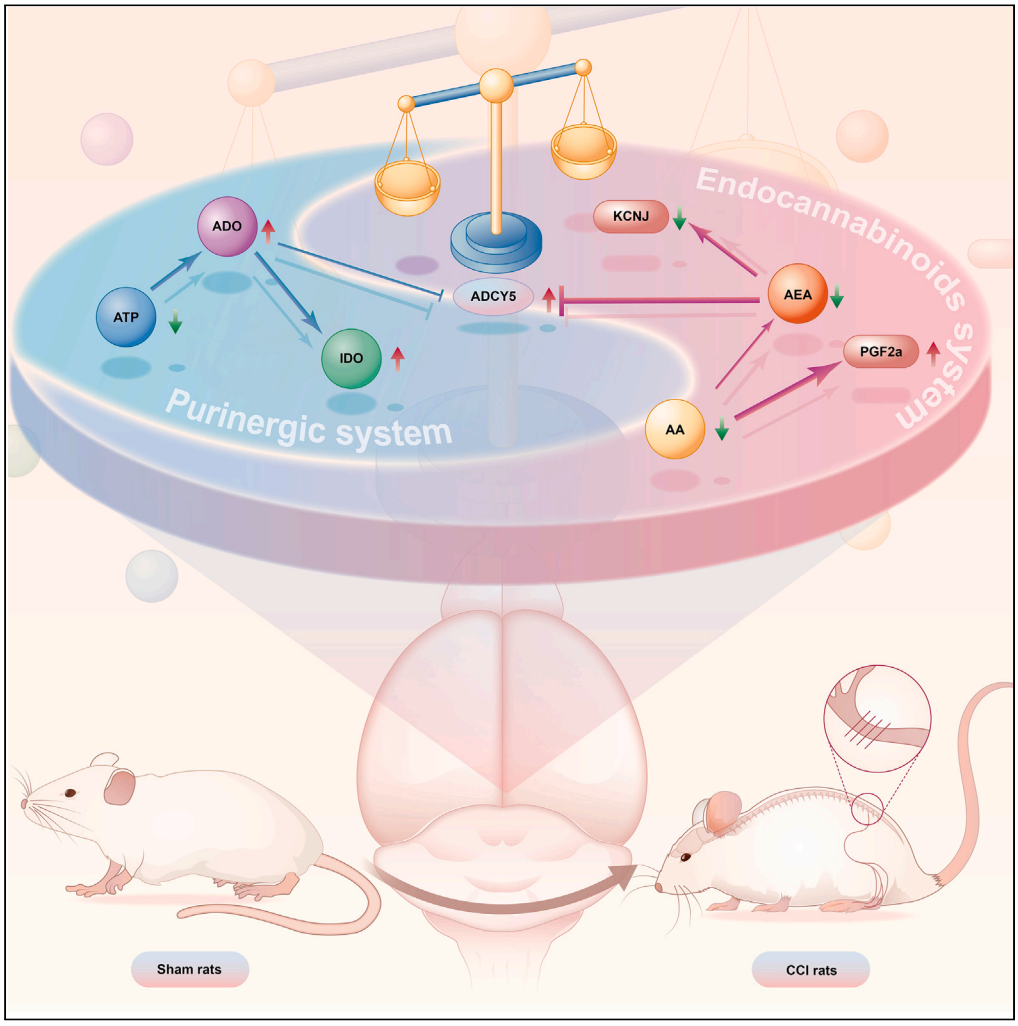

Peng Chen, Chen Wang, Qian Gong, ..., Cuiwen Song, Yuanhua Wu, Long Wang

740466982@qq.com (P.C.)
957269860@qq.com (Y.W.)
wanglongsdu1226@163.com (L.W.)

Highlights

NeP alters the metabolism in the cerebral cortex of CCI rats

NeP causes abnormal expression of proteins in the cerebral cortex of CCI rats

NeP leads to the alterations of endocannabinoids system and purinergic system

Chen et al., iScience 26, 106668
May 19, 2023
https://doi.org/10.1016/j.isci.2023.106668

iScience

CellPress
OPEN ACCESS

Article

Alterations of endogenous pain-modulatory system of the cerebral cortex in the neuropathic pain

Peng Chen,[1,6,7,*] Chen Wang,[2,6] Qian Gong,[3,6] Yihui Chai,[1] Yunzhi Chen,[1] Cuiwen Song,[1] Yuanhua Wu,[4,*] and Long Wang[5,*]

SUMMARY

Neuropathic pain (NeP) remains a significant clinical challenge owing to insufficient awareness of its pathological mechanisms. We elucidated the aberrant metabolism of the cerebral cortex in NeP induced by the chronic constriction injury (CCI) using metabolomics and proteomics analyses. After CCI surgery, the values of MWT and TWL markedly reduced and maintained at a low level. CCI induced the significant dysregulation of 57 metabolites and 31 proteins in the cerebral cortex. Integrative analyses showed that the differentially expressed metabolites and proteins were primarily involved in alanine, aspartate and glutamate metabolism, GABAergic synapse, and retrograde endocannabinoid signaling. Targeted metabolomics and western blot analysis confirmed the alterations of some key metabolites and proteins in endogenous pain-modulatory system. In conclusion, our study revealed the alterations of endocannabinoids system and purinergic system in the CCI group, and provided a novel perspective on the roles of endogenous pain-modulatory system in the pathological mechanisms of NeP.

INTRODUCTION

Neuropathic pain (NeP) is formally defined as pain induced by a lesion or disease of the somatosensory nervous system and commonly characterized by ongoing burning pain, paroxysmal pain, allodynia, and hyperalgesia.[1,2] Data from epidemiological studies show that approximately 6.9%–10% of the general population experience neuropathic pain due to stroke, spinal cord or brain trauma, diabetes, multiple sclerosis, infection, cancer, and chemotherapy.[3,4] Currently, pharmacological treatments, such as tricyclic antidepressants, serotonin, and norepinephrine reuptake inhibitors, and gabapentinoids, are effective in less than half of patients.[5] Hence, a deeper study of the pathophysiological mechanisms in neuropathic pain is urgently needed, which is essential for new drug discovery.

Multiple complex mechanisms from the periphery to brain are implicated in neuropathic pain.[4,6] In recent decades, an extensive cortical network has been revealed to play a critical role in the perception and modulation of pain, such as primary somatosensory cortex (S1), anterior cingulate cortex (ACC), and prefrontal cortex (PFC).[7–10] Functional and structural synaptic plasticity in S1 and ACC are viewed as biomarkers for neuropathic pain and characterized as the increase of turnover rate in dendritic spines, changes in spine morphology, and transformation of pyramidal neurons into hyperactivity.[9] PFC is a brain region where it integrates noxious inputs with sensory perception, cognition, and emotion. It critically modulates the pain experience and a large number of comorbidities of painful disease are evoked by PFC changes, structural reorganization of neurons and glia, signal transduction, and cellular metabolism.[11,12]

Recently, some studies have revealed an association between neuropathic pain and metabolic disturbances in the serum, spinal cord, and pain-related brain regions using multiple approaches.[13] Patti et al. reported the dysregulation of sphingomyelin-ceramide metabolism in the dorsal horn of neuropathic pain animal models induced by tibial nerve transection.[14] Juliana found that regulation of cholesterol metabolism in the spinal microglia alleviated neuropathic pain by inhibiting the perpetuation of neuroinflammation.[15] The metabolic alteration caused by neuropathic pain also emerges in brain. For example, Huo et al. found the change of brain metabolic connectivity and network in rodent models of neuropathic pain

[1]Basic Medical School, Guizhou University of Traditional Chinese Medicine, Guiyang 550025, Guizhou, China

[2]Department of Traditional Chinese Medicine, Zhujiang Hospital of Southern Medical University, Guangzhou 510282, Guangdong, China

[3]First Clinical Medical School, Guangzhou University of Chinese Medicine, Guangzhou 510006, Guangdong, China

[4]The First Affiliated Hospital, Guizhou University of Traditional Chinese Medicine, Guiyang 550025, Guizhou, China

[5]School of Pharmacy, Southwest Medical University, Luzhou 646000, Sichuan, China

[6]These author contributed equally

[7]Lead contact

*Correspondence: 740466982@qq.com (P.C.), 957269860@qq.com (Y.W.), wanglongsdu1226@163.com (L.W.)

https://doi.org/10.1016/j.isci.2023.106668

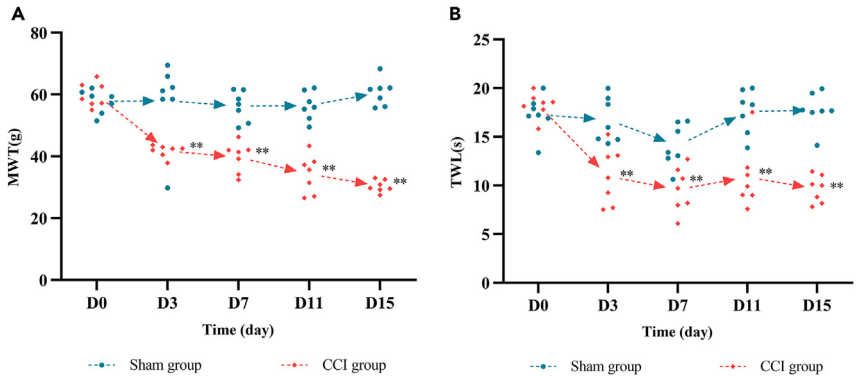

Figure 1. The MWT and TWL values between the CCI group and sham group before and 3, 7, 11, and 15 days after CCI surgery

(A) The MWT values between the CCI group and sham group.

(B) The TWL values between the CCI group and sham group.*$p < 0.05$ and **$p < 0.01$ versus the sham group.

induced by brachial plexus avulsion injury using 2-deoxy-2-[18F] fluoro-D-glucose (18F-FDG) PET images.[16,17] However, the molecular mechanism underlying the phenomena in brain is far from clear.

The chronic constriction injury (CCI) model developed by Bennett and Xie has been a most commonly used model of neuropathic pain caused by peripheral nerve injury.[18] The objective of this study is to investigate the alterations in metabolite and protein expression profiles in the cerebral cortex of the CCI model, with the aim of elucidating the underlying mechanisms involved in the development of neuropathic pain, using proteomic and metabolomic analyses.

RESULTS

CCI caused the changes in pain-related behaviors

As the crucial indicators of pain-related behaviors, mechanical withdrawal threshold (MWT) and thermal withdrawal latency (TWL) are assessed before and 3, 7, 11, and 15 days after CCI surgery. No difference in MWT and TWL values was observed between the sham group and CCI group before surgery ($p < 0.05$) (Figures 1A and 1B). The MWT and TWL values in the CCI group markedly reduced at 3 days after surgery and maintained at a low level during the observation compared with those in the sham group ($p < 0.01$) (Figures 1A and 1B), suggesting that CCI surgery caused significant hyperalgesia.

CCI alters the metabolism in the cerebral cortex

Untargeted metabolomic analyses were used to estimate metabolic disorders in the cerebral cortex triggered by CCI. A total of 816 metabolites in positive ion mode and 605 metabolites in negative ion mode were detected using UHPLC-Q-TOF/MS. Principal component analysis and orthogonal partial least-squares discriminant analysis (OPLS-DA) were performed to analyze the overall distribution and difference between groups (Figures 2A–2D). There was a clear separation between the sham group and CCI group, suggesting alterations of the metabolism in the cerebral cortex induced by neuropathic pain. The results of permutation tests showed the stability and validity of the OPLS-DA model (Figures 2E and 2F).

In the OPLS-DA model, the variable importance in the projection (VIP) value was calculated to explain the importance of each variable to classification. The screening conditions of differentially expressed metabolites (DEMs) were VIP > 1 and $p < 0.05$. In total, 57 DEMs (33 upregulated and 24 downregulated) were screened out in the CCI group compared with the sham group (Figure 3A). Based on the chemical taxonomy, the DEMs largely belong to the classes of amino acids, peptides, and analogs, carbohydrates and carbohydrate conjugates, and fatty acid esters (Figure S1A).

Kyoto Encyclopedia of Genes and Genomes (KEGG) pathway analysis was performed to elucidate the biological functions of DEMs. The enrichment analysis revealed that the DEMs mainly involved in alanine, aspartate and glutamate metabolism, carbon metabolism, biosynthesis of amino acids, phospholipase

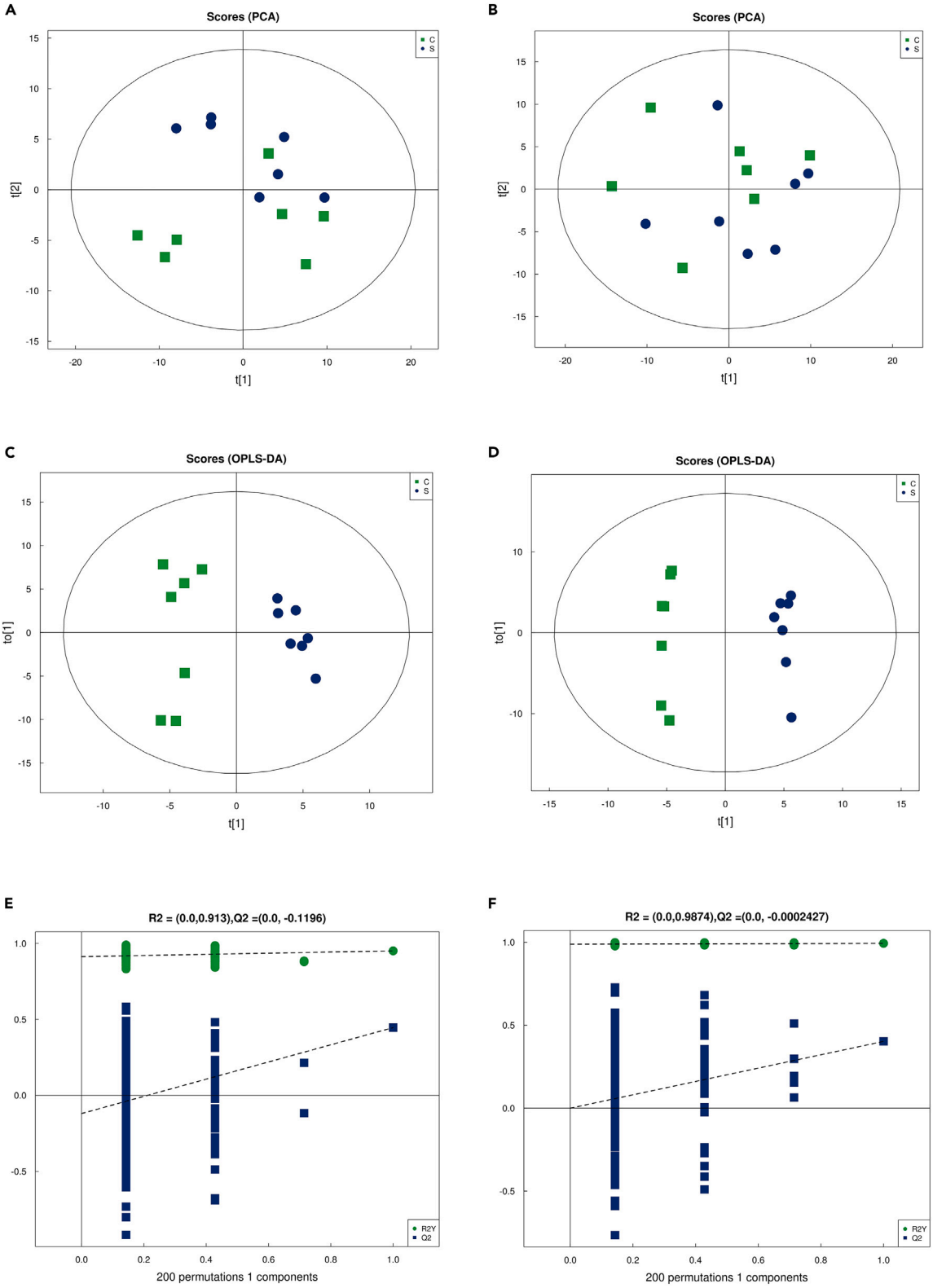
A
Scores (PCA)
t[2]
t[1]
C
S
B
Scores (PCA)
t[2]
t[1]
C
S
C
Scores (OPLS-DA)
to[1]
t[1]
C
S
D
Scores (OPLS-DA)
to[1]
t[1]
C
S
E
R2 = (0.0,0.913),Q2 =(0.0, -0.1196)
R2Y
Q2
200 permutations 1 components
F
R2 = (0.0,0.9874),Q2 =(0.0, -0.0002427)
R2Y
Q2
200 permutations 1 components

Figure 2. PCA score plots, OPLS-DA score plots, and permutation tests in cerebral cortex samples between the CCI (C) and sham (S) groups in the positive and negative ion modes

(A and B) PCA score plots in the positive and negative ion modes.

(C and E) OPLS-DA score plots and permutation tests in positive ion modes.

(D and F) OPLS-DA score plots and permutation tests in negative ion modes.

D signaling pathway, arginine biosynthesis, glucagon signaling pathway, phenylalanine, tyrosine and tryptophan biosynthesis, pentose phosphate pathway, lysosome, and purine metabolism (Figures 3B and S1B). Pearson's correlation analysis was conducted to determine the correlation of DEMs and visualized using a heatmap, with the red and blue color representing strong positive and negative correlations ($|r| > 0.8$ and $p < 0.05$) (Figure S2). For instance, the level of inosine had a significant positive correlation with the abundances of alpha−Linolenic acid, 7-acetoxy-3-formylchromone, and 3-deoxy-*d*-glycero-*d*-galacto-2-nonulosonic acid. These data demonstrate that CCI can cause metabolic disorder in the cerebral cortex.

CCI causes abnormal expression of proteins in the cerebral cortex

Tandem mass tag quantitative proteomic analysis was applied to determine abnormal expression of proteins in the cerebral cortex induced by CCI. Based on the screening conditions of $|FC| \geq 1.2$ and p value < 0.05, 31 differentially expressed proteins (DEPs) were identified in the CCI group compared with the sham group, including 19 upregulated and 12 downregulated proteins (Figures 4A and 4B). The DEPs between the CCI and sham groups were primarily located in the nuclear, cytoplasm, and plasma membrane predominantly located in nucleus, extracellular region, cytoplasm, plasma membrane, and mitochondria (Figure S3A).

Gene ontology annotation was used to classify the cellular component, molecular function (MF), and biological process (BP) of the DEPs between the CCI and sham groups (Figure S3B). For MF, the DEPs were predominantly enriched in oxidoreductase activity, saccharopine dehydrogenase activity, 8-hydroxy-2′-deoxyguanosine DNA binding, forked DNA-dependent helicase activity, telomeric D loop binding, and so on (Figure 4C). For BP, the DEPs were mainly involved in regulation of response to interferon-gamma, interferon-gamma-mediated signaling pathway, humoral immune response mediated by circulating immunoglobulin, alpha-amino acid biosynthetic process, positive regulation of tyrosine phosphorylation of STAT protein, and so on (Figure 4C). The enrichment analysis of KEGG showed that the DEPs were closely related to lysine degradation, D-glutamine and D-glutamate metabolism, nitrogen metabolism, GABAergic synapse, and arginine biosynthesis (Figure 4D).

Integrative analyses of DEMs and DEPs between the CCI and sham groups

An integrative analysis was performed to clarify the relationship between proteins and metabolites. Based on KEGG database, 11 shared pathways of DEMs and DEPs were found, including neuroactive ligand−receptor interaction, alanine, aspartate and glutamate metabolism, lysine degradation, GABAergic synapse, arginine biosynthesis, glycerophospholipid metabolism, and retrograde endocannabinoid signaling (Figures 5A and 5B). The correlation between DEMs and DEPs was calculated using Pearson correlation coefficient and constructed into a correlation network with $|r| \geq 0.8$ and $P < 0.05$ (Figures 5C and 5D). In addition, IPA was applied to categorize the DEMs and DEPs into two functional networks, including "cell cycle, cell-to-cell signaling and interaction, post-translational modification" and "developmental disorder, hereditary disorder, and metabolic disease" (Score > 20, Figures S4 and S5).

CCI alters endogenous pain-modulatory system in the cerebral cortex

Alterations of some key metabolites and proteins in endogenous pain-modulatory system, such as retrograde endocannabinoid signaling and purine metabolism, were found based on the above bioinformatic analysis, and then validated using targeted metabolomics and western blot analysis. The results showed that CCI significantly decreased the levels of ATP, indosine-5′-triphosphate, deoxyguanosine-5′-triphosphate, arachidonic acid, arachidonoyl ethanolamide (AEA), and linoleate, while increased the levels of adenosine and inosine (INO) ($P < 0.05$) (Figure 6). At the protein level, the expression of cyclooxygenase 2, prostaglandin (PG) F2alpha synthase (FAM213B), and adenylate cyclase (ADCY) was elevated in CCI model, while the content of potassium voltage-gated channel (KCNJ) was reduced ($P < 0.05$, Figure 6). These proteins were the key enzyme in the production of PGs from arachidonic acid and the downstream molecules of AEA and adenosine receptors, respectively.

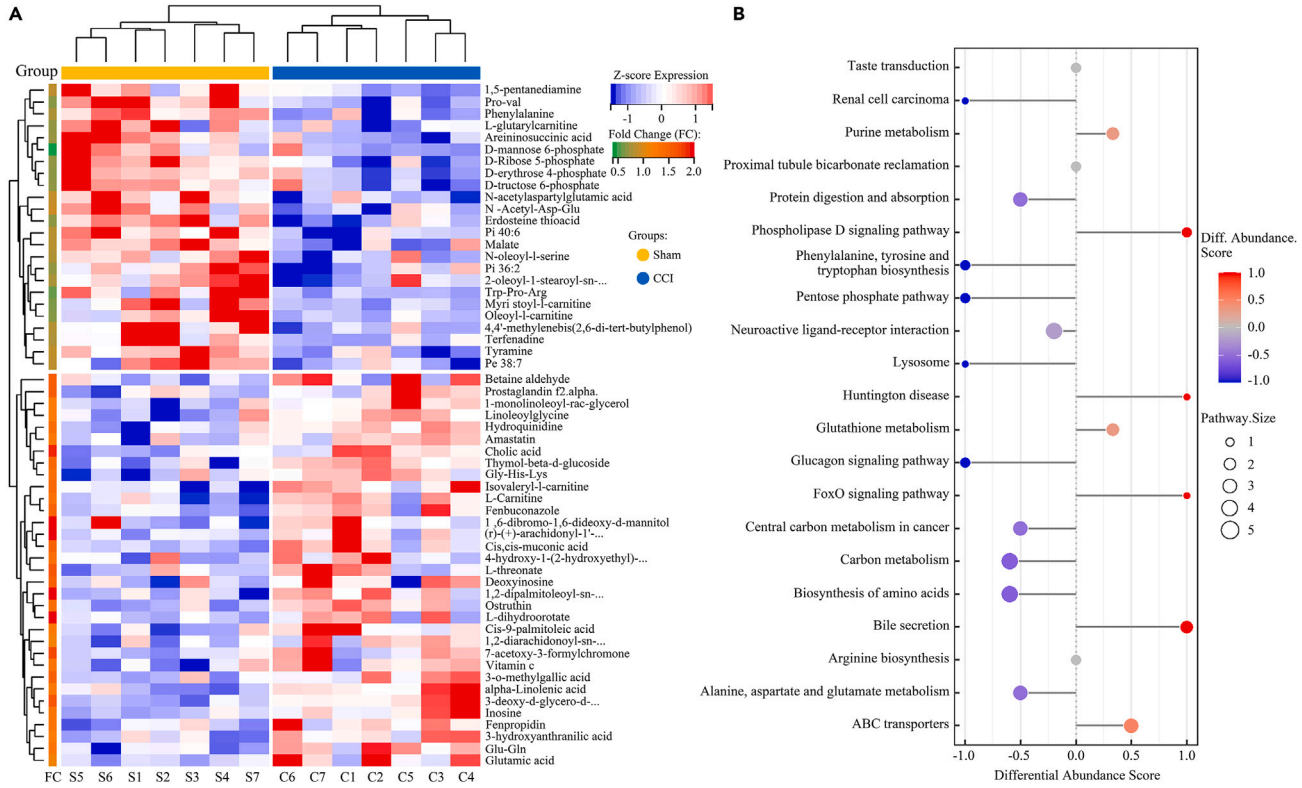

Figure 3. Bioinformation analysis of the DEMs in cerebral cortex samples between the CCI and sham groups

(A) The clustering heatmap of the DEMs in cerebral cortex samples between the CCI and sham groups.

(B) The KEGG enrichment analysis of DEMs in cerebral cortex samples between the CCI and sham groups. See also Figures S1 and S2.

DISCUSSION

The extensive network of the cerebral cortex is considered to play an essential role in the perception and modulation of pain.[7] NeP is almost invariably accompanied by the structural, functional, and metabolic alterations in the pain-related cortical areas.[9,19] In turn, these changes further promote the progression of neuropathic pain. At present, the metabolic mechanism underlying the changes was rarely reported in the cerebral cortex of neuropathic pain.

In this study, we elucidated the aberrant metabolism in the cerebral cortex induced by CCI using the proteomics and metabolomics analyses. For metabolomics analysis, NeP caused significant alterations of 57 metabolites (33 upregulated and 24 downregulated) in the cerebral cortex of the CCI rats, which were enriched in some important pain-related pathways including alanine, aspartate and glutamate metabolism, biosynthesis of amino acids, and purine metabolism. For proteomics analysis, NeP induced aberrant expression of 31 proteins (19 upregulated and 12 downregulated) in the cerebral cortex. Integrative analyses between proteomics and metabolomics showed that DEMs and DEPs were primarily involved in alanine, aspartate and glutamate metabolism, lysine degradation, GABAergic synapse, arginine biosynthesis, glycerophospholipid metabolism, and retrograde endocannabinoid signaling. Finally, targeted metabolomics and western blot further confirmed that retrograde endocannabinoid signaling and purine metabolism were the most important pathways in the regulation and progression of NeP.

AEA is one of the best-characterized endocannabinoids that acts in regulating pain sensation and serves as analgesics in several pain models and clinical neuropathies.[20,21] AEA is classically hydrolyzed from N-acyl-phosphatidylethanolamine by specific phospholipase D and arachidonic acid and ethanolamine by fatty acid amid hydrolase.[22] Arachidonic acid can be metabolized into PG that mostly acts as important mediators of inflammatory response and pain.[23,24] The analgesic effect of AEA in the central nervous system is tightly associated with the cannabinoid receptor 1 (CBR1), which is widely expressed at presynaptic neurons in the cerebral cortex.[21,25] Typically, stimulation of CBR1 inhibits the activity of adenylyl cyclase and protein kinase A, regulates diverse ion

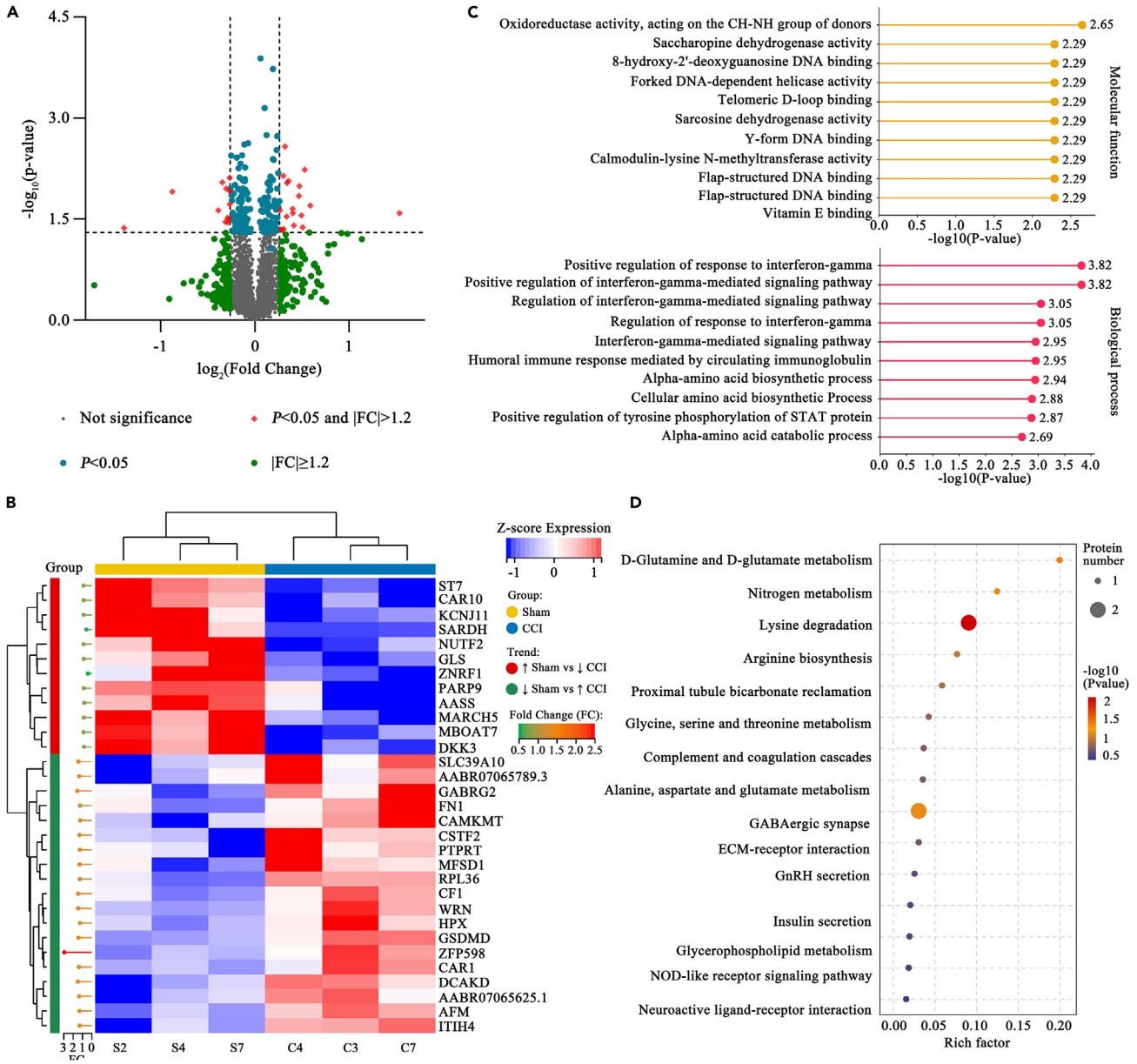

Figure 4. Bioinformation analysis of the DEPs in cerebral cortex samples between the CCI and sham groups

(A) Volcano plots of the DEPs in cerebral cortex samples between the CCI and sham groups.

(B) Clustering heatmaps of the DEPs in cerebral cortex samples between the CCI and sham groups.

(C) GO enrichment analysis of the DEPs in cerebral cortex samples between the CCI and sham groups.

(D) KEGG pathway enrichment analysis of the DEPs in cerebral cortex samples between the CCI and sham groups. See also Figure S3.

channels, and activates several mitogen-activated protein kinases to modulate pain transmission.[26–28] In our study, we found a significant reduction in levels of AEA, arachidonic acid, and linoleic acid, the precursor of arachidonic acid, and varying degrees of elevation in PG by metabolomics analyses. And the results of proteomics and western blot analysis revealed the decrease of KCNJ3 and the increase of ADCY5 and FAM213B. Therefore, we speculated that the excessive synthesis of PG led to the depletion of arachidonic acid and AEA, and abnormal changes of endocannabinoid signaling in neuropathic pain.

The purinergic system, involving ATP and its metabolite adenosine, exerts a critical role in pain generation and transmission.[29] Adenosine is mainly produced by hydrolysis of adenine nucleotides or S-adenosylhomocysteine

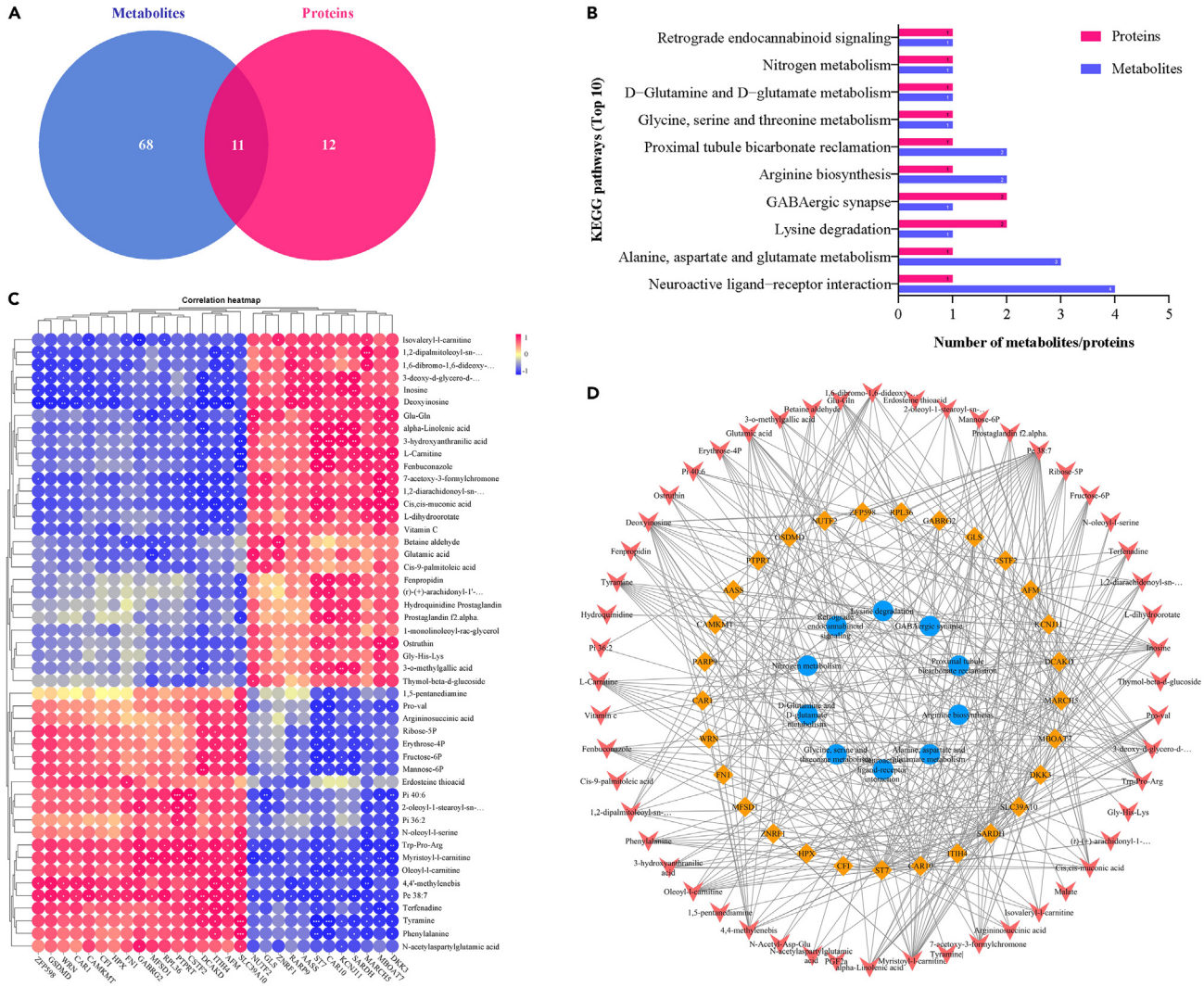

Figure 5. Integrative analyses of DEMs and DEPs in cerebral cortex samples between the CCI and sham groups

(A and B) The shared significant KEGG enrichment pathway of DEMs and DEPs in cerebral cortex samples between the CCI and sham groups.

(C and D) Correlation of DEMs and DEPs in cerebral cortex samples between the CCI and sham groups. See also Figures S4 and S5.

via a series of enzymes.[30] The generation of adenosine is strictly regulated by the metabolic state of cells. Physiologically, adenosine maintains in the low nanomolar range, but markedly increases during the states of heightened metabolic demand, including epilepsy, pain, inflammation, and cancer.[31] Adenosine primarily acts on A1 and A3 adenosine receptors to suppress astrocyte activation, inhibits proinflammatory cytokine expression, and restores GABAergic inhibitory function in the cerebral cortex of neuropathic pain model.[29,32] Inosine, the first metabolite of adenosine, can also induce antinociceptive effect via adenosine A1 receptor.[33,34] In our study, the content of energy molecules, including ATP, GTP, and dGTP, was reduced to varying degrees and the levels of adenosine and inosine were significantly elevated in CCI model, indicating that CCI initiated excessive consumption of energy in the cerebral cortex and stimulated endogenous adenosine system for analgesia to exert a "guardian angel" role.[31]

The endocannabinoids system and purinergic system has been reported to have complex interactions in the past. ATP is usually synthesized in large quantities at the site of tissue injury, and mobilize the release of arachidonic acid and PGE2.[35] Feedback regulation also occurs between multiple pairs of molecules in two systems. Arachidonic acid increases tonic adenosine modulation as a possible feedback loop to limit arachidonic acid facilitation of neuronal excitability.[36] Both AEA and adenosine play inhibitory roles in pain signals downstream of ATP.[37–39] In the development of neuropathic pain, multiple pain and analgesic

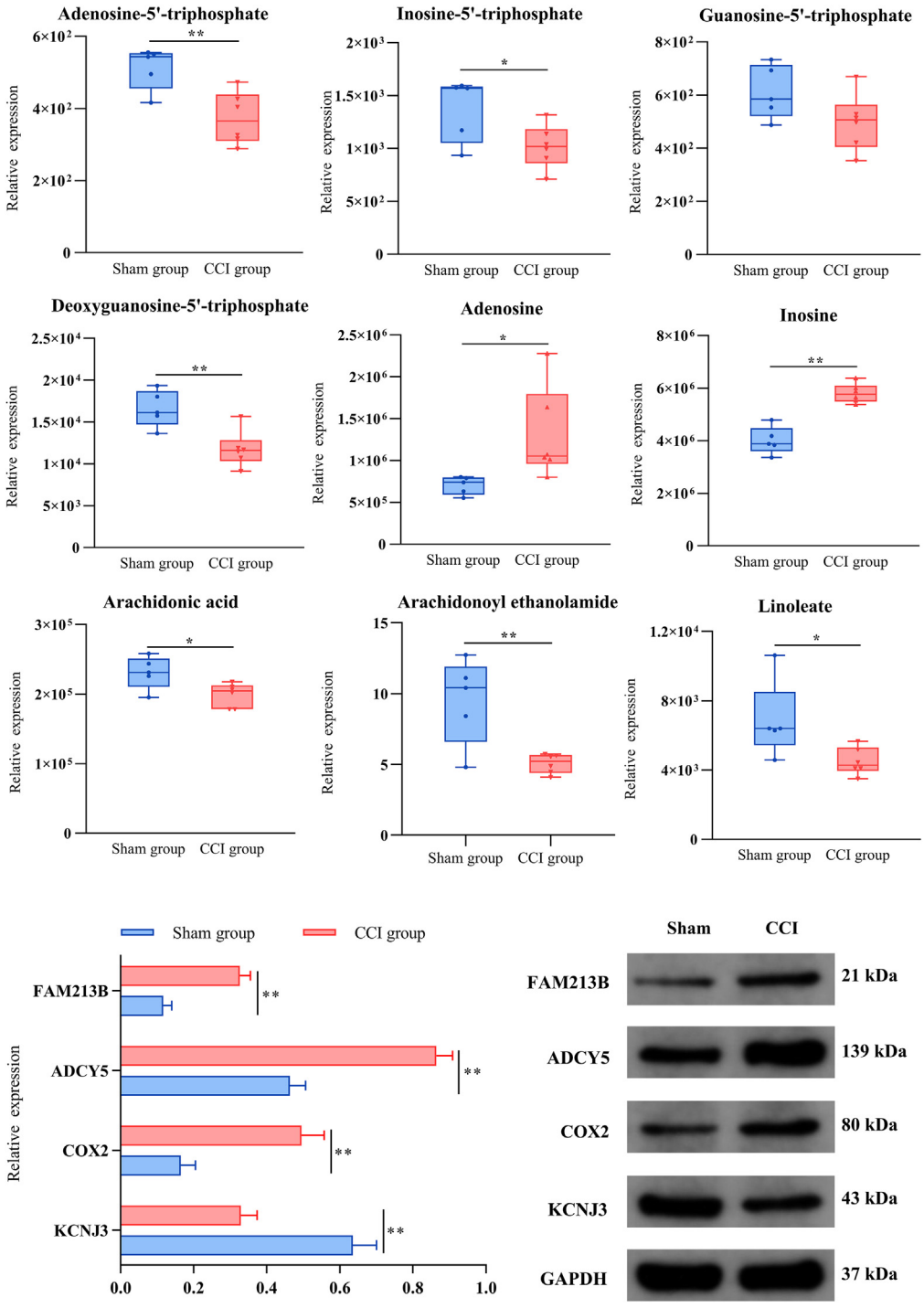

Figure 6. Targeted metabolomics and western blot analysis of key DEMs and DEPs in cerebral cortex samples between the CCI and sham groups

*p < 0.05 and **p < 0.01 versus the sham group.

pathways are disordered, resulting in pathological hyperalgesia. Taking our research findings as an example, the two systems showed opposite trends in the classical analgesic pathway in the CCI model (Figure 7). The depletion of AEA relieves the inhibition of ACDY5, making ATP further trigger downstream pain pathways. However, inhibition of this process by adenosine is not sufficient to reverse the upregulation of

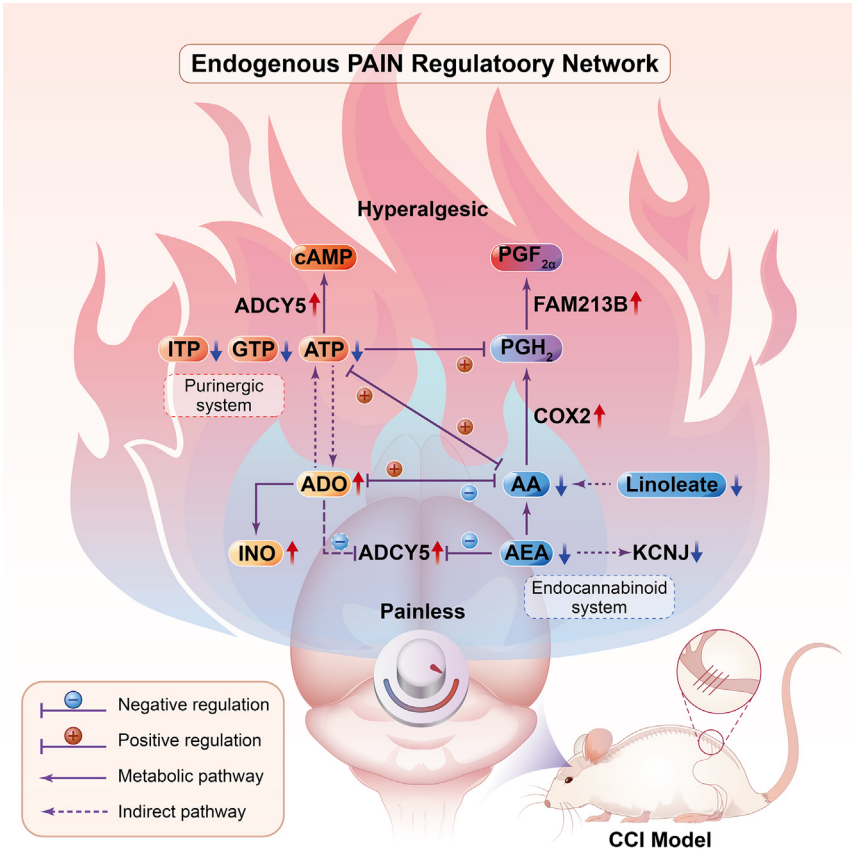

Figure 7. Endogenous pain regulation network

The network mainly contains the endocannabinoids system and purinergic system, which showed opposite trends in the classical analgesic pathway in the CCI model. The "guardian angel" role of endogenous adenosine system can be not enough to extinguish the "painful flame" of hyperalgesia induced by the depletion of AEA.

ACDY5. The role of "guardian angel" may be not enough to extinguish the "painful flame" of hyperalgesia. Based on the above findings, we speculate that the treatment of hyperalgesia caused by neuropathic pain requires more understanding of endogenous pain regulatory networks (such as in-depth analysis of the multi omics), and it is possible to reduce individual pathological feelings through multi-point intervention.

In conclusion, we demonstrate the alterations of endocannabinoids system and purinergic system in CCI-induced NeP using metabolomics and proteomics analyses. Our study provides a novel perspective on the potential roles of endogenous pain-modulatory system in the pathological mechanisms of NeP.

Limitations of the study

This study provided a novel perspective on the potential roles of endogenous pain-modulatory system in the pathological mechanisms of NeP. Unfortunately, we are unable to measure the changes of biochemical and metabolic response at different time points, which is important to obtain a more comprehensive understanding of the pathway sequence and the dynamics of energy demand in NeP.

STAR★METHODS

Detailed methods are provided in the online version of this paper and include the following:

- KEY RESOURCES TABLE
- RESOURCE AVAILABILITY
  - Lead contact
  - Materials availability

SUPPLEMENTAL INFORMATION

Supplemental information can be found online at https://doi.org/10.1016/j.isci.2023.106668.

ACKNOWLEDGMENTS

We thank Shuai Ye of Fudan University for help with our study. This work was supported by Grants from Guizhou Science and Technology Foundation (ZK 2021] General 544) and the National Natural Science Foundation of China (82104658). 2021 Science and Technology Fund Project of Health Commission of Guizhou Province (gzwkj2021-031).

AUTHOR CONTRIBUTIONS

P.C., L.W., and Y.W. designed the research. P.C., C.W., and Q.G. wrote the paper. L.W. and Q.G. performed the experiments. Yi.C. and Yu.C. performed the data analysis. Y.W. and C.S. revised the paper. All the authors have approved the manuscript.

DECLARATION OF INTERESTS

The authors declare no competing interest.

Received: January 18, 2023
Revised: March 23, 2023
Accepted: April 11, 2023
Published: April 13, 2023

REFERENCES

1. Jensen, T.S., Baron, R., Haanpää, M., Kalso, E., Loeser, J.D., Rice, A.S.C., and Treede, R.D. (2011). A new definition of neuropathic pain. Pain *152*, 2204–2205. https://doi.org/10.1016/j.pain.2011.06.017.

2. Truini, A. (2017). A review of neuropathic pain: from diagnostic tests to mechanisms. Pain Ther. *6*, 5–9. https://doi.org/10.1007/s40122-017-0085-2.

3. van Hecke, O., Austin, S.K., Khan, R.A., Smith, B.H., and Torrance, N. (2014). Neuropathic pain in the general population: a systematic review of epidemiological studies. Pain *155*, 654–662. https://doi.org/10.1016/j.pain.2013.11.013.

4. Alles, S.R.A., and Smith, P.A. (2018). Etiology and pharmacology of neuropathic pain. Pharmacol. Rev. *70*, 315–347. https://doi.org/10.1124/pr.117.014399.

5. Finnerup, N.B., Attal, N., Haroutounian, S., Mcnicol, E., Baron, R., Dworkin, R.H., Gilron, I., Haanpää, M., Hansson, P., Jensen, T.S., et al. (2015). Pharmacotherapy for neuropathic pain in adults: a systematic review and meta-analysis. Lancet Neurol. *14*, 162–173. https://doi.org/10.1016/S1474-4422(14)70251-0.

6. Colloca, L., Ludman, T., Bouhassira, D., Baron, R., Dickenson, A.H., Yarnitsky, D., Freeman, R., Truini, A., Attal, N., Finnerup, N.B., et al. (2017). Neuropathic pain. Nat. Rev. Dis. Prim. *3*, 17002. https://doi.org/10.1038/nrdp.2017.2.

7. Xie, Y.F., Huo, F.Q., and Tang, J.S. (2009). Cerebral cortex modulation of pain. Acta Pharmacol. Sin. *30*, 31–41. https://doi.org/10.1038/aps.2008.14.

8. Tan, L.L., and Kuner, R. (2021). Neocortical circuits in pain and pain relief. Nat. Rev. Neurosci. *22*, 458–471. https://doi.org/10.1038/s41583-021-00468-2.

9. Bak, M.S., Park, H., and Kim, S.K. (2021). Neural plasticity in the brain during neuropathic pain. Biomedicines *9*, 624. https://doi.org/10.3390/biomedicines9060624.

10. Bliss, T.V.P., Collingridge, G.L., Kaang, B.K., and Zhuo, M. (2016). Synaptic plasticity in the anterior cingulate cortex in acute and chronic pain. Nat. Rev. Neurosci. *17*, 485–496. https://doi.org/10.1038/nrn.2016.68.

11. Shiers, S., and Price, T.J. (2020). Molecular, circuit, and anatomical changes in the prefrontal cortex in chronic pain. Pain *161*, 1726–1729. https://doi.org/10.1097/j.pain.0000000000001897.

12. Ujcikova, H., Robles, D., Yue, X., Svoboda, P., Lee, Y.S., and Navratilova, E. (2022). Time-Dependent changes in protein composition of medial prefrontal cortex in rats with neuropathic pain. Int. J. Mol. Sci. *23*, 955. https://doi.org/10.3390/ijms23020955.

13. Chen, P., Wang, C., Ren, Y.N., Ye, Z.J., Jiang, C., and Wu, Z.B. (2021). Alterations in the gut microbiota and metabolite profiles in the context of neuropathic pain. Mol. Brain *14*, 50. https://doi.org/10.1186/s13041-021-00765-y.

14. Patti, G.J., Yanes, O., Shriver, L.P., Courade, J.P., Tautenhahn, R., Manchester, M., and Siuzdak, G. (2012). Metabolomics implicates altered sphingolipids in chronic pain of neuropathic origin. Nat. Chem. Biol. *8*, 232–234. https://doi.org/10.1038/nchembio.767.

15. Navia-Pelaez, J.M., Choi, S.H., Dos Santos Aggum Capettini, L., Xia, Y., Gonen, A., Agatisa-Boyle, C., Delay, L., Gonçalves Dos Santos, G., Catroli, G.F., Kim, J., et al. (2021). Normalization of cholesterol metabolism in spinal microglia alleviates neuropathic pain. J. Exp. Med. *218*, e20202059. https://doi.org/10.1084/jem.20202059.

16. Huo, B.B., Zheng, M.X., Hua, X.Y., Shen, J., Wu, J.J., and Xu, J.G. (2021). Metabolic brain network analysis with (18)F-FDG PET in a rat model of neuropathic pain. Front. Neurol. *12*, 566119. https://doi.org/10.3389/fneur.2021.566119.

17. Huo, B.B., Shen, J., Hua, X.Y., Zheng, M.X., Lu, Y.C., Wu, J.J., Shan, C.L., and Xu, J.G. (2019). Alteration of metabolic connectivity in a rat model of deafferentation pain: a 18F-FDG PET/CT study. J. Neurosurg. *132*, 1295–1303. https://doi.org/10.3171/2018.11.JNS181815.

18. Bennett, G.J., and Xie, Y.K. (1988). A peripheral mononeuropathy in rat that produces disorders of pain sensation like those seen in man. Pain *33*, 87–107. https://doi.org/10.1016/0304-3959(88)90209-6.

19. Hubbard, C.S., Khan, S.A., Xu, S., Cha, M., Masri, R., and Seminowicz, D.A. (2015). Behavioral, metabolic and functional brain changes in a rat model of chronic neuropathic pain: a longitudinal MRI study. Neuroimage *107*, 333–344. https://doi.org/10.1016/j.neuroimage.2014.12.024.

20. Watkins, B.A. (2018). Endocannabinoids, exercise, pain, and a path to health with aging. Mol. Aspect. Med. *64*, 68–78. https://doi.org/10.1016/j.mam.2018.10.001.

21. Donvito, G., Nass, S.R., Wilkerson, J.L., Curry, Z.A., Schurman, L.D., Kinsey, S.G., and Lichtman, A.H. (2018). The endogenous cannabinoid system: a budding source of targets for treating inflammatory and neuropathic pain. Neuropsychopharmacology *43*, 52–79. https://doi.org/10.1038/npp.2017.204.

22. Simard, M., Archambault, A.S., Lavoie, J.P.C., Dumais, É., Di Marzo, V., and Flamand, N. (2022). Biosynthesis and metabolism of endocannabinoids and their congeners from the monoacylglycerol and N-acyl-ethanolamine families. Biochem. Pharmacol. *205*, 115261. https://doi.org/10.1016/j.bcp.2022.115261.

23. Bosma, K.J., Kaiser, C.E., Kimple, M.E., and Gannon, M. (2022). Effects of arachidonic acid and its metabolites on functional Beta-Cell mass. Metabolites *12*, 342. https://doi.org/10.3390/metabo12040342.

24. Regulska, M., Szuster-Głuszczak, M., Trojan, E., Leśkiewicz, M., and Basta-Kaim, A. (2021). The emerging role of the Double-Edged impact of arachidonic acid- derived eicosanoids in the neuroinflammatory background of depression. Curr. Neuropharmacol. *19*, 278–293. https://doi.org/10.2174/1570159X18666200807144530.

25. Njoo, C., Agarwal, N., Lutz, B., and Kuner, R. (2015). The cannabinoid receptor CB1 interacts with the WAVE1 complex and plays a role in actin dynamics and structural plasticity in neurons. PLoS Biol. *13*, e1002286. https://doi.org/10.1371/journal.pbio.1002286.

26. Zou, S., and Kumar, U. (2018). Cannabinoid receptors and the endocannabinoid system: signaling and function in the central nervous system. Int. J. Mol. Sci. *19*, 833. https://doi.org/10.3390/ijms19030833.

27. Busquets-García, A., Bolaños, J.P., and Marsicano, G. (2022). Metabolic messengers: endocannabinoids. Nat. Metab. *4*, 848–855. https://doi.org/10.1038/s42255-022-00600-1.

28. Campos, R.M.P., Aguiar, A.F.L., Paes-Colli, Y., Trindade, P.M.P., Ferreira, B.K., de Melo Reis, R.A., and Sampaio, L.S. (2021). Cannabinoid therapeutics in chronic neuropathic pain: from animal research to human treatment. Front. Physiol. *12*, 785176. https://doi.org/10.3389/fphys.2021.785176.

29. Zhou, M., Wu, J., Chang, H., Fang, Y., Zhang, D., and Guo, Y. (2023). Adenosine signaling mediate pain transmission in the central nervous system. Purinergic Signal. *19*, 245–254. https://doi.org/10.1007/s11302-021-09826-2.

30. Fredholm, B.B. (2007). Adenosine, an endogenous distress signal, modulates tissue damage and repair. Cell Death Differ. *14*, 1315–1323. https://doi.org/10.1038/sj.cdd.4402132.

31. Borea, P.A., Gessi, S., Merighi, S., and Varani, K. (2016). Adenosine as a Multi-Signalling guardian angel in human diseases: when, where and how does it exert its protective effects? Trends Pharmacol. Sci. *37*, 419–434. https://doi.org/10.1016/j.tips.2016.02.006.

32. Shaw, S., Uniyal, A., Gadepalli, A., Tiwari, V., Belinskaia, D.A., Shestakova, N.N., Venugopala, K.N., Deb, P.K., and Tiwari, V. (2020). Adenosine receptor signalling: probing the potential pathways for the ministration of neuropathic pain. Eur. J. Pharmacol. *889*, 173619. https://doi.org/10.1016/j.ejphar.2020.173619.

33. Nascimento, F.P., Macedo-Júnior, S.J., Pamplona, F.A., Luiz-Cerutti, M., Córdova, M.M., Constantino, L., Tasca, C.I., Dutra, R.C., Calixto, J.B., Reid, A., et al. (2015). Adenosine A1 receptor-dependent antinociception induced by inosine in mice: pharmacological, genetic and biochemical aspects. Mol. Neurobiol. *51*, 1368–1378. https://doi.org/10.1007/s12035-014-8815-5.

34. Nascimento, F.P., Figueredo, S.M., Marcon, R., Martins, D.F., Macedo, S.J., Lima, D.A.N., Almeida, R.C., Ostroski, R.M., Rodrigues, A.L.S., and Santos, A.R.S. (2010). Inosine reduces pain-related behavior in mice: involvement of adenosine A1 and A2A receptor subtypes and protein kinase C pathways. J. Pharmacol. Exp. Therapeut. *334*, 590–598. https://doi.org/10.1124/jpet.110.166058.

35. Xia, M., and Zhu, Y. (2011). Signaling pathways of ATP-induced PGE2 release in spinal cord astrocytes are EGFR transactivation-dependent. Glia *59*, 664–674. https://doi.org/10.1002/glia.21138.

36. Cunha, R.A., Almeida, T., and Ribeiro, J.A. (2000). Modification by arachidonic acid of extracellular adenosine metabolism and neuromodulatory action in the rat hippocampus. J. Biol. Chem. *275*, 37572–37581. https://doi.org/10.1074/jbc.M003011200.

37. Howlett, A.C., Breivogel, C.S., Childers, S.R., Deadwyler, S.A., Hampson, R.E., and Porrino, L.J. (2004). Cannabinoid physiology and pharmacology: 30 years of progress. Neuropharmacology *47*, 345–358. https://doi.org/10.1016/j.neuropharm.2004.07.030.

38. Burnstock, G. (2008). Purinergic signalling and disorders of the central nervous system. Nat. Rev. Drug Discov. *7*, 575–590. https://doi.org/10.1038/nrd2605.

39. Effendi, W.I., Nagano, T., Kobayashi, K., and Nishimura, Y. (2020). Focusing on adenosine receptors as a potential targeted therapy in human diseases. Cells *9*, 785. https://doi.org/10.3390/cells9030785.

40. Victorino, A.B., Serra, F.T., Piñero, P.P., de Almeida, A.A., Lopim, G.M., Matias Junior, I., Machado, H.R., Lent, R., Cabral, F.R., Gomez-Pinilla, F., et al. (2017). Aerobic exercise in adolescence results in an increase of neuronal and non-neuronal cells and in mTOR overexpression in the cerebral cortex of rats. Neuroscience *361*, 108–115. https://doi.org/10.1016/j.neuroscience.2017.08.002.

41. Herculano-Houzel, S., and Lent, R. (2005). Isotropic fractionator: a simple, rapid method for the quantification of total cell and neuron numbers in the brain. J. Neurosci. *25*, 2518–2521. https://doi.org/10.1523/JNEUROSCI.4526-04.2005.

42. Gu, Z., Li, L., Tang, S., Liu, C., Fu, X., Shi, Z., and Mao, H. (2018). Metabolomics reveals that crossbred dairy buffaloes are more thermotolerant than holstein cows under chronic heat stress. J. Agric. Food Chem. *66*, 12889–12897. https://doi.org/10.1021/acs.jafc.8b02862.

43. Wiśniewski, J.R., Zougman, A., Nagaraj, N., and Mann, M. (2009). Universal sample preparation method for proteome analysis. Nat. Methods *6*, 359–362. https://doi.org/10.1038/nmeth.1322.

STAR★METHODS

KEY RESOURCES TABLE

REAGENT or RESOURCE	SOURCE	IDENTIFIER
Antibodies		
Rabbit anti-KCNJ3	Affinity	Cat# AF9101; RRID: AB_2843292
Rabbit anti-ADCY5	Bioss	Cat# bs-3922R; RRID: AB_10857032
Rabbit anti-FAM213B	Abcam	Cat# Ab180932
Rabbit anti-COX2	Affinity	Cat# AF7003; RRID: AB_2835311
Anti-GDNF antibody	Good Here Biotech	Cat# AB-P-R 001
Goat anti–rabbit horseradish peroxidase (HRP)	Wuhan Boster Biological Technology	Cat# BA1054; RRID: AB_2734136
Chemicals, peptides, and recombinant proteins		
Methanol	Fisher Scientific	Cat# A456-4
Acetonitrile	Merck	Cat# 1499230-935
Ammonium acetate	Merck	Cat# 70221
Ammonium hydroxide	Fisher Scientific	Cat# A470-500
Ammonium formate	Merck	Cat# 70221
Formic acid	Merck	Cat# 00940
Sodium dodecyl sulfate (SDS)	Bio-Rad	Cat# 161-0302
Dithiothreitol	Merck	Cat# 9163-5G
Trypsin	Promega	Cat# V5113
KH2PO4	Sinopharm	Cat# 10017618
KCl	Sinopharm	Cat# 10016318
RIPA lysis buffer	Meilunbio	Cat# MA0151
Protease inhibitors	Meilunbio	Cat# MB12707
PVDF membrane	Millipore	Cat# IPVH00010
Critical commercial assays		
Isotope standards	Cambridge Isotope Laboratories	N/A
BCA protein assay	Biyuntian	Cat# P0012
TMT reagent	Thermo Scientific	N/A
Experimental models: Organisms/strains		
Rat: Sprague-Dawley	Hunan SJA Laboratory Animal Co.	N/A
Software and algorithms		
SPSS Statistics	https://www.ibm.com/support/pages/downloading-ibm-spss-statistics-27	Version 27.0.
KASS	http://www.genome.jp/kegg/kaas/	Version 2.0
Proteome Discoverer	Thermo Scientific	Version 1.4
MASCOT	Matrix Science	Version 2.2
Others		
Electronic von Frey anaesthesiometer	IITC Life Science	Model: 38450
Paw stimulator analgesia meter	IITC Life Science	Model: 390
UHPLC system	Agilent Technologies	Model: 1290 Infinity
Triple TOF 6600 mass spectrometer	AB Sciex	Model: Triple TOF 6600
6500+ QTRAP mass spectrometer	AB Sciex	Model: QTRAP 6500+
C18 column	Waters	Model: ACQUITY UPLC BEH C18

(*Continued on next page*)

Continued

REAGENT or RESOURCE	SOURCE	IDENTIFIER
Amide column	Waters	Model: ACQUITY UPLC BEH Amide
Centrifuge	Eppendorf	Model: 5430R
Empore™ SPE Cartridges C18	Merck	Cat# 66883-U
AKTA Purifier system	GE Healthcare	Model: Purifier100
Q-Exactive mass spectrometer	Thermo Scientific	Model: Q-Exactive HF-X
Acclaim PepMap100	Thermo Scientific	N/A
EASY column	Thermo Scientific	N/A

RESOURCE AVAILABILITY

Lead contact

Requests for further information or materials should be directed to the lead contact Peng Chen (740466982@qq.com).

Materials availability

This study did not generate new unique reagents.

Data and code availability

- All data reported in this paper will be shared by the lead contact on request.
- This paper does not report original code.
- Any additional information required to reanalyze the data reported in this paper is available from the lead contact on request.

EXPERIMENTAL MODEL AND SUBJECT DETAILS

Animals

Sprague-Dawley rats (male, six weeks old, 160-200g) were obtained from Hunan SJA Laboratory Animal Co., Ltd, (Changsha, China; Certificate NO. SCXK (Xiang) 2019-0004) and maintained in specific pathogen-free (SPF) facility with a 12-hour light/dark cycle and a liberalized diet. Fourteen rats were randomized into the sham group and CCI group (n=7 in each group). Animal experimental design and procedures were reviewed and approved by Animal Use and Ethic Committee of the First Affiliated Hospital of Guangzhou University of Chinese Medicine (License No. GZTCMF1-2018037).

METHOD DETAILS

Animal models

The rats were anaesthetized with pentobarbitone sodium for preparation of CCI surgery in reference to the previous literature.[13] The skin of the left thigh was incised and the local muscles were separate to adequately expose the sciatic nerve. The nerve was moderately ligated by making four thread knots using 4-0 silk with a 1 mm separation between each knot. In parallel, the rats in the sham group underwent the same surgical steps without ligation.

Behavioral tests

Mechanical withdrawal threshold (MWT) and thermal withdrawal latency (TWL) were performed to evaluate mechanical and thermal hyperalgesia before surgery and 3, 7, 11 and 15 days after surgery. For MWT test, the rats were individually acclimated to the environment in a transparent plexiglass box with a mental metal mesh floor for 30 min. The ipsilateral plantar surface of the rats was stimulated using an electronic von Frey anaesthesiometer (IITC Life Science Instruments, Woodland Hills, CA, USA) five times at five-minute intervals. For TWL test, the rats were individually acclimated to the environment in transparent plastic boxes for 30 min. A radiant heat source (Model 390, IITC Life Science Instruments, Woodland Hills, CA, USA) was focused on the surface of the left hindpaw. When the rats lifted or licked the hindpaw, the corresponding figures on the screen were documented and averaged to obtain MWT and TWL values.

Sample preparation

At day 15 after surgery, the animals were intraperitoneally injected with pentobarbitone sodium (40 mg/kg) and heavily anaesthetized. In accordance with standard anatomical landmarks, we carefully separated the cerebral cortex from whole brain tissue of rats to investigate this region.[40,41] Specifically, we used the following method: 1) Following decapitation, the rat's skull was carefully removed, and the brain was extracted while being kept on ice; 2) The cerebral cortex was then separated from the whole brain by peeling it away along the midline on the surface of the brain. The hippocampus, located at the base of the cerebral cortex, was clearly visible and was not included in our dissection; 3) It's important to note that the cerebral cortex is composed of gray matter, while the subcortical cortex is composed of white matter, and these regions were readily distinguishable with the naked eye. Cerebral cortical tissues were harvested, immediately frozen in liquid nitrogen and stored at -80°C for ultraperformance liquid chromatography/quadrupole time-of-flight mass spectrometry (UPLC-Q-TOF-MS) and liquid chromatography-tandem mass spectrometry (LC-MS/MS).

Untargeted metabolomics analysis

The cerebral cortex samples were homogenized three times (20s each) in 200 μL of H_2O with five ceramic beads by the homogenizer. The homogenized solution was added with 800 μL of pre-cooled methanol/acetonitrile (1:1 volume ratio) and centrifuged for 15 min (14000 g, 4°C) to take the supernatant and dry it in a vacuum centrifuge.

For untargeted metabolomics analysis, LC-MS/MS were conducted with an Agilent1290 Infinity UHPLC system (Agilent Technologies, Santa Clara, CA, USA) coupled to a Sciex TripleTOF 6600 instrument (AB Sciex, Foster City, CA, USA). Hydrophilic interaction liquid chromatography (HILIC) separation was performed using an ACQUITY UPLC BEH column (2.1 mm×100 mm, 1.7 μm; Waters, Manchester, UK) with the injection volume of 2 μL, the flow rate of 0.3 mL/min and the column temperature of 25°C. The mobile phase consisted of buffer A (25 mM ammonium acetate + 25 mM ammonium hydroxide + water) and buffer B (acetonitrile) with a linear gradient as follows: 85% buffer B for 1 min, a linear decrease of buffer B from 85% to 65% for 11 min, a decrease of buffer B from 65% to 40% for 0.1 min, 40% buffer B for 4 min, and a rapid increase of buffer B from 40% to 85% for 0.1 min.

MS analysis was carried out in electrospray ionization (ESI) negative and positive modes and the conditions were set as follows: ion source gas1 (GS1) 60 psi, ion source gas2 (GS2) 60 psi, curtain gas (CUR) 30 psi, temperature 600°C, and ion spray voltage (IS) ±5500 V. MS acquisition was performed in a range of 60-1000 Da with the accumulation time of 0.20 s/spectra. MS/MS acquisition was performed in a range of 25-1000 Da with the accumulation time of 0.05 s/spectra. The product ion scan is acquired using information dependent acquisition (IDA) model with the collision energy of 35 V ± 15 eV, declustering potential of ±60 V, exclude isotopes within 4 Da, and 10 candidate ions to monitor per cycle.

The raw MS data were converted and imported into XCMS software for peak picking, peak grouping, annotation of isotopes and adducts. The metabolites were identified by comparing accuracy m/z value (<25 ppm) and MS/MS spectra with an in-house database which was established with available authentic standards.[42] After sum-normalization, the processed data were subjected to multivariate data analysis, such as principal component analysis (PCA) and orthogonal partial least-squares discriminant analysis (OPLS-DA). In the OPLS-DA model, the variable importance in the projection (VIP) value of each variable was calculated to explain its contribution to classification. Furthermore, univariate analyses were conducted to determine the differences between the sham and CCI groups. VIP > 1 and $P < 0.05$ were used as the screening criteria of differentially expressed metabolites (DEMs). Hierarchical clustering of samples and DEMs was performed using ComplexHeatmap *R* package (Version 3.4). Kyoto Encyclopedia of Genes and Genomes (KEGG) pathway annotations were carried out using KEGG Automatic Annotation Server (KASS, http://www.genome.jp/kegg/kaas/). Pearson correlations of DEMs were conducted using a free online platform (https://www.bioinformatics.com.cn).

Proteomics analysis

Sample lysis and protein extraction were performed with SDT buffer, including 4% sodium dodecyl sulfate (SDS), 100 mM Tris-HCl (pH7.6) and 1 mM dithiothreitol (DTT). Protein was quantified with the bicinchoninic acid (BCA) protein assay (Biyuntian, Shanghai, China) and digested by trypsin using the filter-aided sample preparation (FASP) method.[43] The digested peptides were desalted using Empore™ SPE Cartridges C18

(Sigma, St Louis, MO, USA), concentrated by vacuum centrifugation and redissolved in 40 μL of 0.1% formic acid. The peptide content was determined with UV light spectral density at 280 nm. To each sample, approximately 100 μg peptides mixture was labeled using tandem mass tag (TMT) reagent (Thermo Scientific, Waltham, MA, USA) based on the manufacturer's instructions.

The fractionation of the labeled peptides was carried out by strong cation exchange chromatography with the AKTA Purifier system (GE Healthcare, Piscataway, NJ, USA). Buffer A was 10 mM KH_2PO_4 in 25% of acetonitrile (pH 3.0), buffer B was 500 mM KCl and 10 mM KH_2PO_4 in 25% of acetonitrile (pH 3.0). The peptides mixture was reconstituted with buffer A, injected into a Polysulfoethyl column (4.6 mm×100 mm, 5 μm, 200 Å; PolyLC Inc, Maryland, USA), and separated at a flow rate of 1 mL/min with a linear gradient as follows: 0% buffer B for 25 min, 0–10% buffer B for 7 min, 10%-20% buffer B for 10 min, 20-45% buffer B for 5 min, 45%–100% buffer B for 5 min, and 100% buffer B for 8 min. The collected fractions were further desalted and concentrated by vacuum centrifugation.

For proteomics analysis, LC-MS/MS were conducted with a Q-Exactive mass spectrometer (Thermo Scientific) coupled to Easy nLC (Thermo Scientific). The peptides were loaded onto an Acclaim PepMap100 nano column (100 μm×2 cm; Thermo Scientific) and separated by a C18-reversed phase analytical column (75 μm×10 cm; Thermo Scientific) at the flow rate 300 nl/min. Buffer A was 0.1% Formic acid, and buffer B was 0.1% formic acid in 84% acetonitrile with a linear gradient. MS analysis was carried out in the positive ion mode. MS data was obtained in a data-dependent method by dynamically selecting the top 10 most abundant precursor ions for high energy collision dissociation (HCD) fragmentation. The conditions were set as follow: automatic gain control target 3e6, maximum inject time 10 ms, dynamic exclusion duration 40.0 s, survey scans at a resolution of 70,000 at m/z 200, HCD spectra at a resolution of 17,500 at m/z 200, isolation window 2 m/z, normalized collision energy 30 eV, and underfill ratio 0.1%.

The raw MS data were analyzed by the MASCOT engine (Version 2.2; Matrix Science, London, UK) and Proteome Discoverer 1.4 software. Related parameters and instructions were set as follows: trypsin as the enzyme, 2 maximum missed cleavages, peptide mass tolerance as ±20 ppm, fragment mass tolerance as 0.1 Da, and peptide false discovery rate (FDR) as ≤0.01. Only unique peptides were used for protein quantification. Normalization was performed based on protein intensity values. |fold change (FC)| ≥1.2 and $p<0.05$ were defined as the screening criteria of differentially expressed proteins (DEPs). Hierarchical clustering of samples and DEPs was performed using ComplexHeatmap R package (Version 3.4). Protein subcellular localization was predicted with CELLO (http://cello.life.nctu.edu.tw/). Gene ontology (GO) annotation and KEGG pathway annotation were conducted separately using Blast2GO software (https://www.blast2go.com/) and KEGG Automatic Annotation Server with enrichment analysis performed by the Fisher' exact tests.

Association analysis

All DEMs and DEPs were queried and mapped to KEGG pathways and enrichment analysis was carried out. R Version 3.5.1 was applied to combine the annotation and enrichment results of KEGG in the two omics, which was visualized by venn diagram and bar plot. Pearson correlation coefficient of DEMs and DEPs were calculated via an online Omicshare Tools (https://www.omicshare.com/tools/) and loaded into Cytoscape software (Version 3.7.2) to conduct a correlation network. Ingenuity pathway analysis (IPA, http://www.ingenuity.com/) software was used to categorize the DEMs and DEPs into two functional networks.

Targeted metabolomics analysis

The samples were added with 1000 μL of cold methanol/acetonitrile/water (2:2:1 volume ratio) solvent and stock solutions of stable-isotope internal standards, adequately vortexed and homogenized, sonicated at 4°C and then centrifuged for 20 min (14000 g, 4°C) to take the supernatant and dry it in a vacuum centrifuge at 4°C. For LC-MS/MS analysis, the samples were redissolved in 100 μL acetonitrile/water (1:1 volume ratio) and centrifuged for 15 min (14000 g, 4°C) to collect the supernatant.

Analyses were conducted with the Agilent1290 Infinity UHPLC system coupled to a quadrupole linear ion trap mass spectrometer (QTRAP 6500+, AB Sciex, Foster City, CA, USA). HILIC separation and reversed-phase liquid chromatography (RPLC) separation were performed respectively using the UPLC BEH Amide and C18 columns (2.1mm×100mm, 1.7 μm; Waters, Manchester, UK) with the injection volume of 2 μL. For HILIC separation, the mobile phase was composed of buffer A (90% H2O + 2 mM ammonium formate +

10% acetonitrile) and buffer B (0.4% formic acid + methanol) with a gradient as follows: 85% buffer B for 1 min, 85%-80% buffer B for 2 min, 80% buffer B for 1 min, 80%-70% buffer B for 2 min, 70%-50% buffer B for 4 min, 50% buffer B for 5.5 min, 50%-85% buffer B for 0.1 min, and 85% buffer B for 7.4 min at the flow rate of 0.3 mL/min and the column temperature of 35°C. For RPLC separation, mobile phase A was comprised of 5 mM ammonium acetate and 0.2% $NH_3 \cdot H_2O$ in water, and mobile phase B was 0.4% formic acid in methanol with the gradient as follows: 5%-60% buffer B for 5 min, 60%-100% buffer B for 6 min, 100% buffer B for 2 min, 100%-5% buffer B for 0.1 min, and 5% buffer B for 2.9 min at the flow rate of 0.4 mL/min and the column temperature of 40°C.

MS analysis was carried out using the 6500+ QTRAP mass spectrometer in negative and positive modes and the conditions were set as follows: source temperature 580°C, GS1 45 psi, GS2 60 psi, CUR 30 psi, and IS ±4500 V. Multiple reaction monitoring (MRM) method was employed for MS quantitative data acquisition. The quantitative data was processed by MultiQuant to calculate the relative content of metabolite.

Western blot analysis

The total proteins were extracted from cerebral cortex by 1 × RIPA lysis buffer (Meilunbio, Dalian, China) containing protease inhibitors (Meilunbio, Dalian, China) and phosphatase inhibitors (Meilunbio, Dalian, China). A total of 25 μg proteins were separated by sodium dodecyl sulfate-polyacrylamide gel electrophoresis (SDS-PAGE) and transferred to polyvinylidene fluoride (PVDF) membrane. Then the PVDF membrane was in blocked with 5% skim milk powder solution in PBS-Tween 20 (PBST) for 60 min and incubated with primary antibodies overnight at 4°C. After that, the membrane was incubated with secondary antibodies for 40 min at room temperature. The blots were detected using ECL system (Vazyme Biotech, Nanjing, China) and captured by a ChemiDoc MP Imaging System (Bio-Rad, Hercules, CA, USA). The primary antibodies were as follows: KCNJ3 (Affinity, AF9101), ADCY5 (Bioss, bs-3922R), FAM213B (Abcam, Ab180932), and COX2 (Affinity, AF7003).

QUANTIFICATION AND STATISTICAL ANALYSIS

All experimental data were expressed as means ± standard deviations and statistical analyses were performed using IBM SPSS Statistics 27.0. Shapiro-Wilk test and Levene test were respectively used to assess the normality in the distribution of each group and the homogeneity in the variance between the CCI and sham groups. Student's t-test was used for comparisons between the two groups. $P < 0.05$ was statistically significant.